Predicting migration velocity anomalies

Paul J. Fowler

ABSTRACT

In SEP-51 (Fowler, 1987) I derived a linear operator that relates perturbations in interval slownesses to the resultant changes in the migration slownesses observed along dipping reflectors. This operator can be represented as a filtered version of a tomographic back-projection operator. For flat beds it reduces to the stacking slowness operator studied by Toldi (1985). For dipping beds the operator still resembles the flat dip one, but is skewed by the effect of the dip. This behavior can be illustrated clearly using pictures of the operator for a fixed reflecting point in the subsurface. Predictions of changes in migration slowness derived using this linear operator closely match those measured from synthetic data.

INTRODUCTION

Many methods have been used for velocity analysis in structurally complex areas. One leading approach uses tomographic techniques based on fitting a velocity model to measured traveltimes (e.g., Gray and Golden, 1983; Bishop, et al., 1985; Stork and Clayton, 1986; Sword, 1987). Another approach tries to maximize energy in a prestack migration (Al-Yahya, 1987); this last method is a generalization of conventional stacking velocity analysis, in which the energy (or semblance) in a stacked image is maximized. In previous papers (Fowler, 1985, 1986, 1987), I have developed a method that combines aspects of these two approaches by extending the approach used by Toldi (1985) for stacking velocity analysis. I use energy in a prestack migrated image as an objective function to be maximized by best choice of a velocity function. These time-migration velocities can be measured using multiple constant-velocity prestack Stolt migration (Shurtleff, 1984), or by applying DMO and migration to constant-velocity stacks (Fowler, 1984). Migration velocities can be evaluated in this way as readily and robustly as conventional stacking velocities, but are corrected for the structural effects that can drastically bias stacking velocities. The tomographic aspect of this approach enters in using kinematic computations to find a gradient direction to guide the iterative improvement of the velocity model. The heart of this method is the derivation of a linear operator relating perturbations in interval slowness to the resulting changes in prestack time-migration slowness. As I show below, this operator may be viewed as a filtered version of more conventional tomographic back-projection.

Write the migration slowness $\mathbf{w}$ as a function of midpoint y and zero-offset time τ, and the interval slowness $\mathbf{m}$ as a function of lateral position x and depth z. The relation between these two slownesses will generally be complex and nonlinear. Inverting

migration slownesses for interval slownesses thus requires an iterative solution, using an updated linear approximation at each step. What is needed is an expression for $\partial w_d / \partial m_a$, relating a change in interval slowness at a particular model anomaly point $\mathbf{a}=(x_a, z_a)$ to the resulting change in observed migration slowness at some point $\mathbf{d}=(y_d, \tau_d)$ in the data space. That is, one needs a linear operator $\mathbf{G}$ such that

$$\Delta \mathbf{w}(x_d, z_d) = \mathbf{G}\ \Delta \mathbf{m}(x_a, z_a) \tag{1}$$

One complication is immediately apparent. The migration slowness data $w(y_d, \tau_d)$, are a function of the midpoint y and migrated time τ, and not directly of the physical position (x_d, z_d). Hence one needs to know how to relate (x_d, z_d) to (y_d, τ_d). This suggests beginning with a model for which this map is known (such as a homogeneous average background), and updating this map at each iteration by computing changes $\Delta\tau_d$ and Δy_d as well as Δw_d. The operator $\mathbf{G}$ thus has three parts:

$$\begin{bmatrix} \Delta \mathbf{w}_d \\ \Delta \tau_d \\ \Delta \mathbf{y}_d \end{bmatrix} = \begin{bmatrix} \mathbf{G}_\mathbf{w} \\ \mathbf{G}_\tau \\ \mathbf{G}_\mathbf{y} \end{bmatrix} \Delta \mathbf{m} \tag{2}$$

As I discussed in SEP-51 (Fowler, 1987), this operator should be weighted to reflect the dip spectrum present at each point in the data. Picking a single dominant dip corresponds to the usual practice in tomographic inversion of digitizing horizons; using a weighted spectrum of dips allows for the uncertainty with which we can really determine dips from data by "blurring" the back-projection. The dip spectrum can be estimated from the time migrated image extracted from the constant-velocity prestack time migrations using one's best available migration velocity function. These dips will be slopes in migrated time, so as the local estimate of the migration velocity w_d is updated, the conversion to physical dips will also change. Thus, at each iteration the position (x_d, z_d) and dip θ_d corresponding to a point (y_d, τ_d) in the time migrated data will change. In effect, one computes a mapping from a time-migrated image to a depth-migrated image as one iterates away from a laterally invariant velocity model to a laterally varying one, a mapping similar in effect to that found by tracing image rays (Larner, et al., 1981).

FILTERED TOMOGRAPHY

The construction of the operator $\mathbf{G}$ can be split into two parts. The first part finds $\partial t / \partial m$ by tomography, and the second finds $\partial w / \partial t$, $\partial \tau / \partial t$, and $\partial y / \partial t$ by generalized inversion of double-square-root traveltime equations. The operator $\mathbf{G}$ thus decomposes into a tomographic operator $\mathbf{B}$, and a filtering operator $\mathbf{A}^{-g}$:

$$\begin{bmatrix} \Delta \mathbf{w}_d \\ \Delta \tau_d \\ \Delta \mathbf{y}_d \end{bmatrix} = \mathbf{A}^{-g}\, \mathbf{B}\, \Delta \mathbf{m} \tag{3}$$

The operator $\mathbf{A}$ that expresses the double-square-root traveltime equation perturbations is found as a forward operator relating traveltime changes Δt to perturbations in the parameters Δw_d, $\Delta \tau_d$, and Δy_d. The superscript $-g$ is used here to indicate that $\mathbf{A}$ operates in the wrong direction, so that a generalized inverse to $\mathbf{A}$ is what is actually needed.

Relating model perturbations to traveltime perturbations

The computation of traveltimes to a subsurface point given a velocity model is done readily by ray tracing. For a ray S, the traveltime is just the integral along the ray of the slowness m:

$$t = \int_S m \; ds \tag{4}$$

Invoking Fermat's principle, one can perturb the model and calculate the changes in traveltimes integrating the slowness perturbations along the *unperturbed* ray S_{ik}:

$$\Delta t = \int_S \Delta m \; ds = \mathbf{B}\,\Delta\mathbf{m} \tag{5}$$

In discretized form, this gives a linear operator $\mathbf{B}$ relating interval slowness perturbations to travel time changes. For a constant slowness background, this operator can be found analytically, as I showed in SEP-51 (Fowler, 1987). This is a standard computation for a tomographic inversion. However, rather than pick traveltimes and try to invert B to find interval velocities, I use the migration-velocity filter $\mathbf{A}^{-g}$ so that events never need to be picked explicitly, which should be a boon in noisy or complicated data.

Relating traveltime perturbations to diffraction pyramids

Consider first a single point diffractor at (x_d, z_d) in a medium of constant slowness w. If one runs a seismic survey passing over this point, the kinematics of the pre-stack point diffractor are described by the pyramid equation

$$t = w\sqrt{z_d{}^2+(y-h-x_d)^2} + w\sqrt{z_d{}^2+(y+h-x_d)^2} \tag{6}$$

where t, y, and h are the traveltime, the midpoint, and the half-offset specifying an event in a particular trace. Suppose now that the slowness model is perturbed. The travel-time data for the point diffractor are now a set $\{t_{ik}, y_i, h_k\}$ that no longer satisfies equation (1) exactly. However, if the perturbations are not too large, it is possible to define a slowness w_d, a zero-offset time τ_d, and a lateral position x_d for which an equation of the form

$$t = \sqrt{\tau_d^2/4 + w_d{}^2(y-h-y_d)^2} + \sqrt{\tau_d^2/4 + w_d{}^2(y+h-y_d)^2} \tag{7}$$

best fits the data points in a least-squares sense.

One can solve the problem of fitting such a pyramid through the data points $\{t_{ik}, y_i, h_k\}$ by linearizing around an initial value of $(\hat{w}_d, \hat{\tau}_d, \hat{y}_d)$. Then the set of equations to solve are given by

$$\Delta t(y_i, h_k) = t_{ik} - t(\hat{w}_d, \hat{\tau}_d, \hat{y}_d) \approx \frac{\partial t}{\partial w_d}\Delta w_d + \frac{\partial t}{\partial \tau_d}\Delta \tau_d + \frac{\partial t}{\partial y_d}\Delta y_d \tag{8}$$

where all the partial derivatives are evaluated at $(\hat{w}_d, \hat{\tau}_d, \hat{y}_d, y_i, h_k)$. Written as a matrix equation, this becomes

$$\Delta\mathbf{t} \approx \mathbf{A}\begin{bmatrix} \Delta\mathbf{w}_d \\ \Delta\tau_d \\ \Delta\mathbf{y}_d \end{bmatrix} \tag{9}$$

where $\mathbf{A}$ is a matrix of the partial derivatives of t. If a generalized inverse for $\mathbf{A}$ can be found, one can write

$$\begin{bmatrix} \Delta \mathbf{w}_d \\ \Delta \tau_d \\ \Delta \mathbf{y}_d \end{bmatrix} = \mathbf{A}^{-g}\, \Delta \mathbf{t} = \mathbf{A}^{-g}\, \mathbf{B}\, \Delta m \tag{10}$$

which is just the desired decomposition of $\mathbf{G}$.

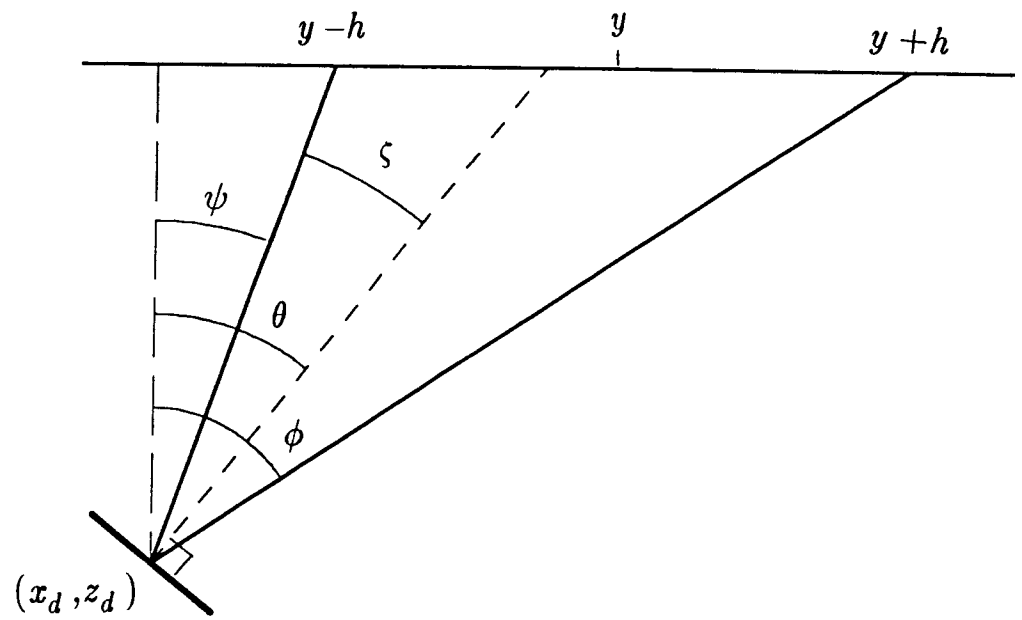

FIG. 1. Geometry of rays for a dipping bed and a constant background slowness. The rays for a single trace with midpoint y and offset h are shown, along with the normal ray (dashed). The reflecting point is at (x_d, z_d). Note that the normal ray does not go through y.

A DEGENERATE DEGREE OF FREEDOM

In SEP-51 (Fowler, 1987) I showed how to decompose the traveltime pyramid into dip components to find $\partial w / \partial m$ for a particular dip θ, and derived an explicit solution for the single-dip operator using a constant-slowness background. In implementing this operator, I found that the matrix $\mathbf{A}$ was persistently singular. Singular value decomposition of $\mathbf{A}$ showed that there was always one singular value that was far smaller than the other two, suggesting that only two of the parameters Δw_d, $\Delta \tau_d$, and Δy_d could be found independently. For the flat bed, this may be understood readily. Explicitly, the

derivatives in equation 8 are given by

$$\begin{bmatrix} t_{w_d} \\ t_{\tau_d} \\ t_{y_d} \end{bmatrix} = \frac{1}{\sqrt{\tau_d^2/4 + w_d^2(y-h-y_d)^2}} \begin{bmatrix} w_d(y-h-y_d)^2 \\ \tau_d/4 \\ w_d^2(y_d-y+h) \end{bmatrix} + \frac{1}{\sqrt{\tau_d^2/4 + w_d^2(y+h-y_d)^2}} \begin{bmatrix} w_d(y+h-y_d)^2 \\ \tau_d/4 \\ w_d^2(y_d-y-h) \end{bmatrix}. \tag{11}$$

where, to make the notation more compact, I denote the partial derivatives by subscripts: $\partial t/\partial w_d \equiv t_{w_d}$, etc. But for flat beds, $y = y_d$ always, and t_{y_d} is identically zero, so there are only two, not three, independent parameters to be found; hence **A** will be singular.

Why is **A** also singular for non-zero dips? Intuitively, the ray picture for migration-velocity analysis looks like that for flat-bed stacking-velocity analysis, but rotated by the dip angle so that the rays remain symmetric around the normal incidence ray. For flat dips one can resolve changes in τ_d, that is, vertical changes, but not changes in y_d along the bed. For the dipping bed it is reasonable to expect that one can similarly resolve changes perpendicular to the bed, but not along it. Specifying a fixed dip angle θ eliminates one degree of freedom in the fitting function and makes it translationally invariant along the dip direction.

Consider using the variables z_d and x_d to fit the traveltime data, where $z_d = \tau_d/2w_d$ and $x_d = y_d$. The partial derivatives are then given by

$$t_{w_d} = w_d \left[\sqrt{z_d^2 + (y-h-x_d)^2} + \sqrt{z_d^2 + (y+h-x_d)^2} \right] \tag{12}$$

$$t_{z_d} = \frac{w_d z_d}{\sqrt{z_d^2 + (y-h-x_d)^2}} + \frac{w_d z_d}{\sqrt{z_d^2 + (y+h-x_d)^2}} \tag{13}$$

$$t_{x_d} = \frac{-w_d(y-h-y_d)}{\sqrt{z_d^2 + (y-h-x_d)^2}} + \frac{-w_d(y+h-y_d)}{\sqrt{z_d^2 + (y+h-x_d)^2}} \tag{14}$$

In terms of the angles ϕ, ψ, θ, and ς in Figure 1, these last two derivatives become

$$\begin{aligned} t_{z_d} &= w_d (\cos\phi + \cos\psi) \\ &= w_d \left[\cos(\theta-\varsigma) + \cos(\theta+\varsigma) \right] \\ &= 2w_d \cos\theta \cos\varsigma \end{aligned} \tag{15}$$

and

$$\begin{aligned} t_{x_d} &= -w_d (\sin\phi + \sin\psi) \\ &= -w_d \left[\sin(\theta-\varsigma) + \sin(\theta+\varsigma) \right] \\ &= -2w_d \sin\theta \cos\varsigma \end{aligned} \tag{16}$$

Thus, if θ is fixed,

$$\frac{t_{x_d}}{t_{z_d}} = -\tan\theta \tag{17}$$

and so Δx_d and Δz_d cannot be found independently. In practice, this means that, no matter what set of parameters is used, only two will be independent, and small singular values of $\mathbf{A}$ will need to be zeroed if three parameters are used in the inversion. Alternatively, $\mathbf{A}$ may be inverted in terms of only two variables, with the third found explicitly from these two.

VISUALIZING THE OPERATOR

The operators $\mathbf{G}_w$, $\mathbf{G}_r$, and $\mathbf{G}_y$ are functions of the four variables x_a, z_a, x_d, and z_d describing the locations of an anomaly **a** and a reflecting point **d**. Four dimensional pictures are difficult for most of us to comprehend. It is easiest to look at the operators either for a fixed anomaly **a** or for a fixed reflecting point **d**. I use the latter approach here. For simplicity, I compute the operators against a background with constant slowness of 0.5 s/km, which is physically of the right magnitude for rocks and conveniently cancels out scaling factors of $2w$. In passing, I note that kilometers and seconds are good units to use here, because distances, times and slownesses will ordinarily then all be of the same magnitude. This is important because the inversion uses parameters with different physical dimensions (slownesses, times, and distances), and the condition number of $\mathbf{A}$ can be adversely affected by poor scaling of units.

Flat bed operators

Figure 2 shows the operator $\mathbf{G}_w$ for a single fixed reflecting point **d** and dip angle θ=0. The point **d** is located at the apex of the triangular region in the figure; one can think of this as isolating for examination one point on a flat bed through this location. The picture then displays the magnitude of change one could one would expect to measure in the migration slowness measured at the point **d** caused by a perturbation in the interval slowness anywhere else. The gray background indicates no change; because of the finite cable aperture, slowness anomalies outside the central triangular region cannot affect the migration slowness at the point **d**. Within the triangular region, light areas indicate positive changes and dark areas negative changes. To clarify this pattern, Figure 3 shows a cross-section along the top of Figure 2. Here, amplitude of $\mathbf{G}_w$ is plotted as a function of x_a with z_a held constant. The pattern of positive response for wide offset rays and negative response for inner offsets can be compared with Figure 4.6 in John Toldi's dissertation (Toldi, 1985) or Figure 2 of Loinger (1983); Toldi also provides good discussion of the origin of this pattern. For flat beds (θ=0), prestack time migration is essentially just normal moveout and stacking, and the operators should be the same. As I showed in SEP-51 (Fowler, 1987), the migration operator I use here does indeed formally reduce to Toldi's stacking slowness operator for flat beds, and numerical testing confirms that they are indistinguishable.[1]

[1] The proof of equivalence of the two operators required the choice of a particular weighting function for the least-squares fitting of the traveltime equations (8). However, numerical testing has convinced me that the operator is remarkably insensitive to the particular choice of weights used.

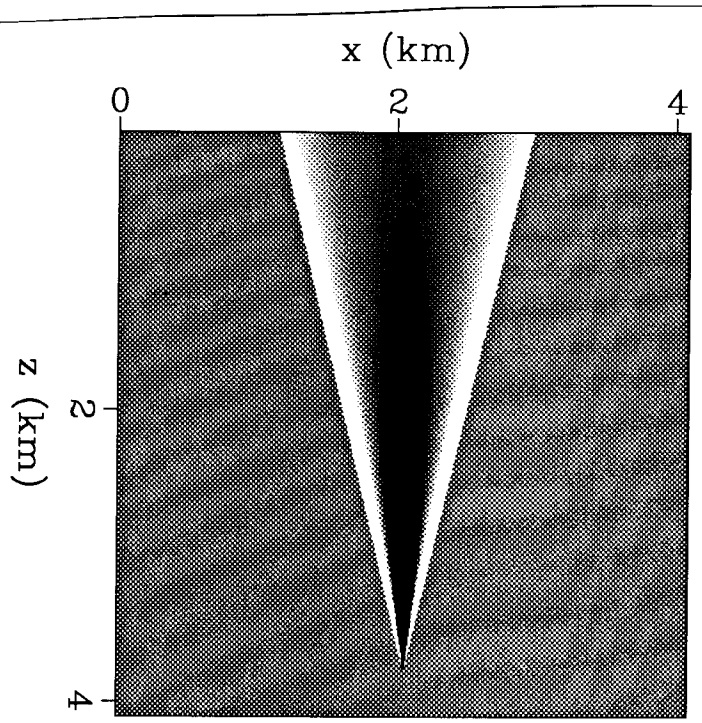

FIG. 2. The operator $\mathbf{G}_w$ for a single fixed reflecting point **d** and dip angle θ=0. The picture displays the magnitude of change in the migration slowness w_d measured at a point **d**, caused by a perturbation in the interval slowness at any other point. The point **d** is located at the apex of the triangular region. The gray background indicates no change; because of the finite cable aperture, the operator is zero outside the central triangular region. Within the triangular region, light areas indicate positive response and dark areas negative response.

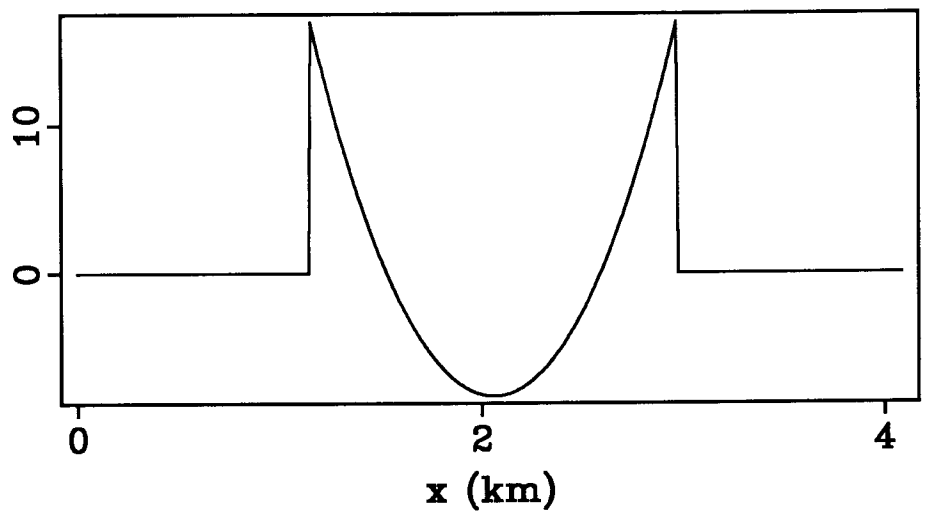

FIG. 3. Amplitude of $\mathbf{G}_w$ for a flat bed, plotted as a function of lateral anomaly position x_a with anomaly depth z_a held constant. This figure corresponds to a cross-section along the top of Figure 2. Wide offset rays show a positive response, and inner offsets a negative response.

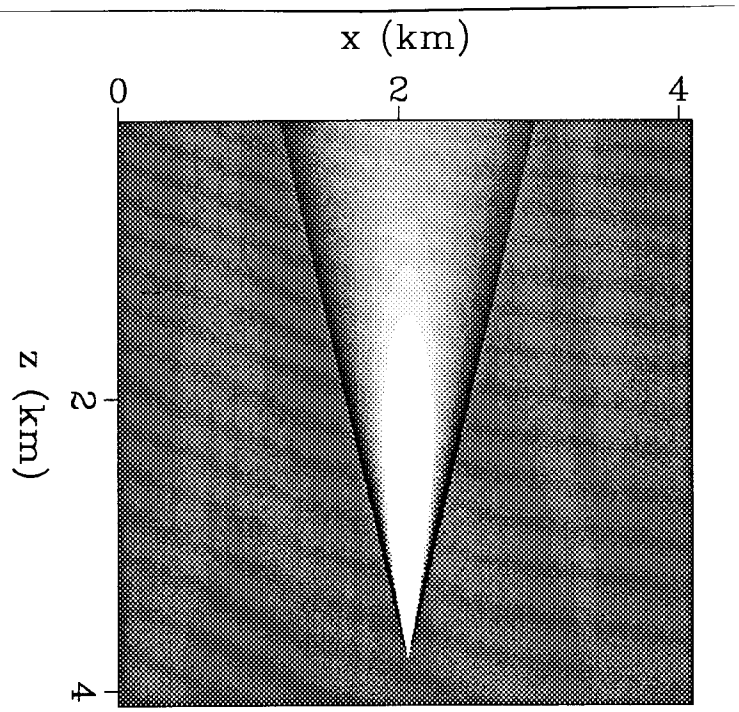

FIG. 4. The operator $\mathbf{G}_\tau$ for a single fixed reflecting point **d** and dip angle θ==0. The picture displays the magnitude of change in the migrated time location τ_d of a point **d**, caused by a perturbation in the interval slowness at any other point. The point **d** is located at the apex of the triangular region. The gray background indicates no change; because of the finite cable aperture, the operator is zero outside the central triangular region. Within the triangular region, light areas indicate positive response and dark areas negative response.

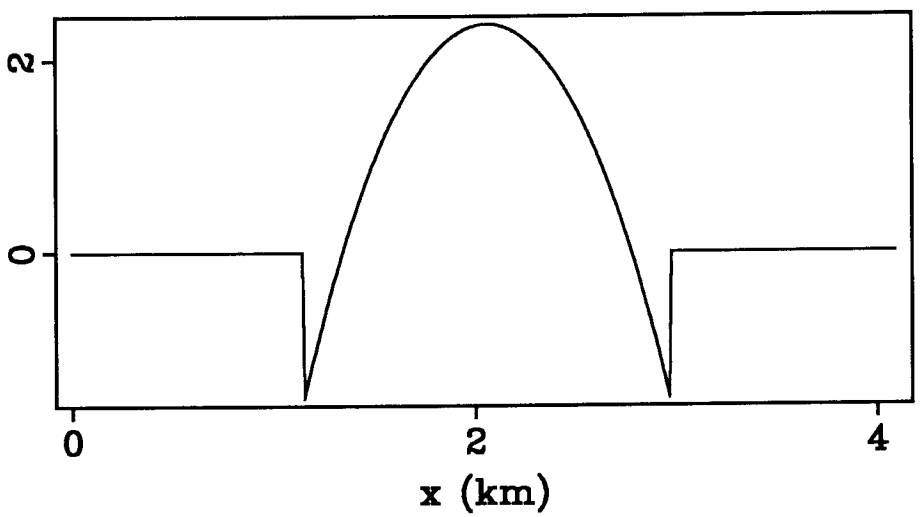

FIG. 5. Amplitude of $\mathbf{G}_\tau$ for a flat bed, plotted as a function of lateral anomaly position x_a with anomaly depth z_a held constant. This figure corresponds to a cross-section along the top of Figure 4. Wide offset rays show a negative response, and inner offsets a positive response, the opposite of the pattern for $\mathbf{G}_w$ in Figure 3.

Figure 4 shows the operator $\mathbf{G}_\tau$ for θ=0. The pattern is similar to that of $\mathbf{G}_w$ in Figure 2 but this time with negative changes at wide offsets and positive changes at inner offsets. Figure 5 again shows a cross-section along the top of Figure 4, graphing the magnitude of $\mathbf{G}_\tau$ for fixed z_a and varying x_a. No figure is shown for $\mathbf{G}_y$, because, as discussed above, it is identically zero for flat beds.

Dipping bed operators

The ray picture in Figure 1 for non-zero dip θ is similar to that for flat beds, but skewed by the dip. Similarly, the operator $\mathbf{G}_w$ for non-zero θ is similar to the flat bed of Figure 2, but again skewed. This operator $\mathbf{G}_w$ for a 30 degree dip is shown in Figure 6, and a cross-section is shown in Figure 7. The pattern of positive response at wide offsets and negative at inner offsets is again seen. Note that the response pattern is now symmetric not around the middle of the aperture, but instead around the normal ray.

Figures 8 and 9 illustrate the operator $\mathbf{G}_\tau$ for θ=30. Again, comparison with the flat bed operators in Figures 4 and 5 show that the dipping-bed migration slowness operator is essentially similar to the flat-bed stacking slowness operator, but skewed by the dip angle.

Figures 10 and 11 display the operator $\mathbf{G}_y$. Because the dip is not zero, this operator is no longer identically zero. As suggested by equation (17), $\mathbf{G}_y$ is proportional to $\mathbf{G}_\tau$.

MODELING THE EFFECTS OF SLOWNESS ANOMALIES

The operator $\mathbf{G}$ discussed above predicts changes in migration slowness for specified perturbations in interval slowness. How good is this prediction? To test this, I created some simple structural models, introduced simple slowness anomalies, and generated synthetic data using finite-difference modeling. I then created pre-stack migrated images using velocity-space DMO and migration (Fowler, 1984), and measured the slownesses at which the images had maximum energy. These results are compared with the slownesses predicted using the $\mathbf{G}_w$ operator applied to the model slowness perturbations.

Figure 12 shows a slowness model containing a flat bed, and above it, a circular anomaly in the background slowness. The slowness in the upper layer is 0.5 s/km, and that in the lower layer is 0.33 km/s. The slowness anomaly has a peak value of 0.476 s/km at the center, and decays as a gaussian function to the background of 0.5 s/km. The zero-offset synthetic data from the finite-difference modeling is shown in Figure 13. A cable length of 1 km was used in the modeling; the model is 4 km long, and the reflecting bed is at a depth of 2 km.

The migration slownesses measured along the flat reflecting bed are shown in Figure 14. The predicted slownesses are overlaid for comparison. The two curves fit well, displaying the same shape and amplitude. Small differences are expected for several reasons. First, I have used a linear approximation to a nonlinear relation. Second, least-squares fitting of traveltimes is not identical to stacking waveforms. Third, the calculation using the linear operator assumes an offset geometry that is invariant for all midpoint, whereas the modeled data have an alternating value for the inner offset, since the shot interval was equal to the geophone spacing. Finally, analysis of migration or stacking slownesses from data ignores the finite length of the wavelet, which introduces a

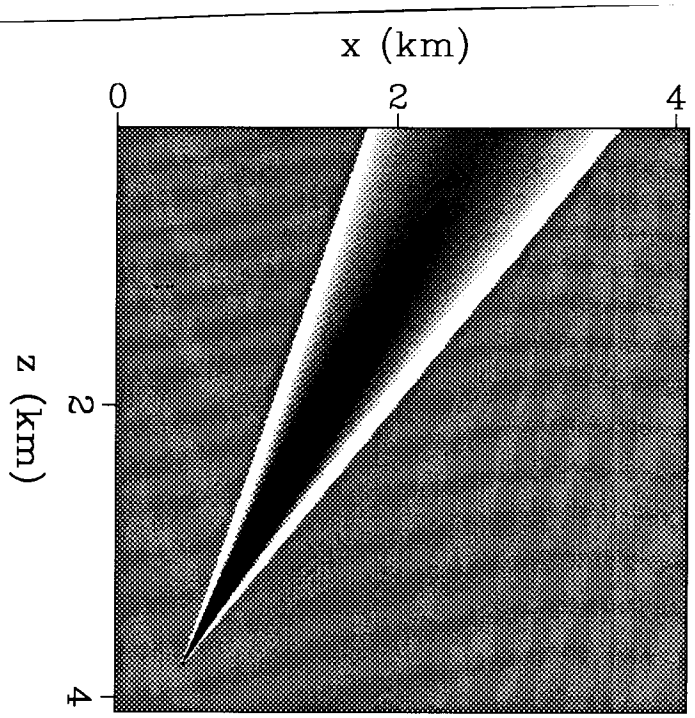

FIG. 6. The operator $\mathbf{G}_w$ for a single fixed reflecting point **d** and dip angle θ=30. The picture displays the magnitude of change in the migration slowness w_d measured at a point **d**, caused by a perturbation in the interval slowness at any other point. The point **d** is located at the apex of the triangular region. The gray background indicates no change; because of the finite cable aperture, the operator is zero outside the central triangular region. Within the triangular region, light areas indicate positive response and dark areas negative response. The operator is similar to the flat dip operator in Figure 2, but skewed by the dip.

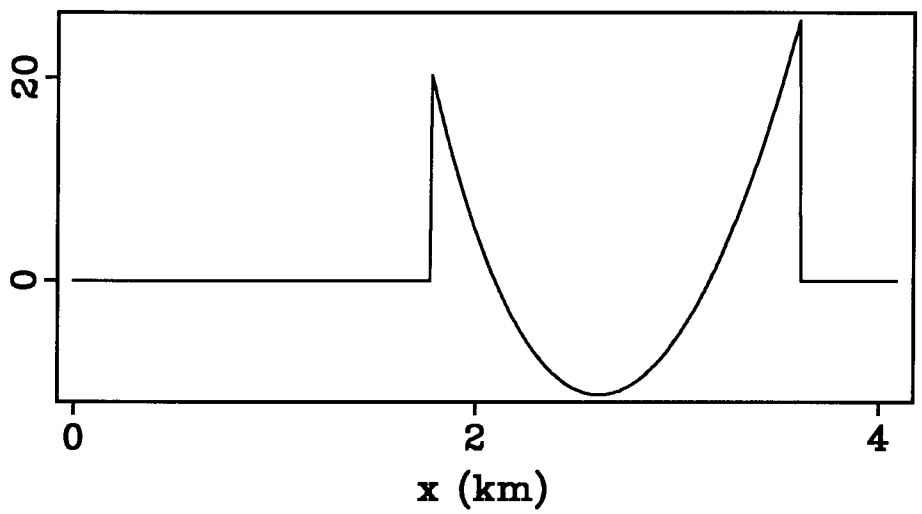

FIG. 7. Amplitude of $\mathbf{G}_w$ for a dipping bed, plotted as a function of lateral anomaly position x_a with anomaly depth z_a held constant. This figure corresponds to a cross-section along the top of Figure 6. Wide offset rays show a positive response, and inner offsets a negative response, similar to that of the flat bed operator in Figure 3.

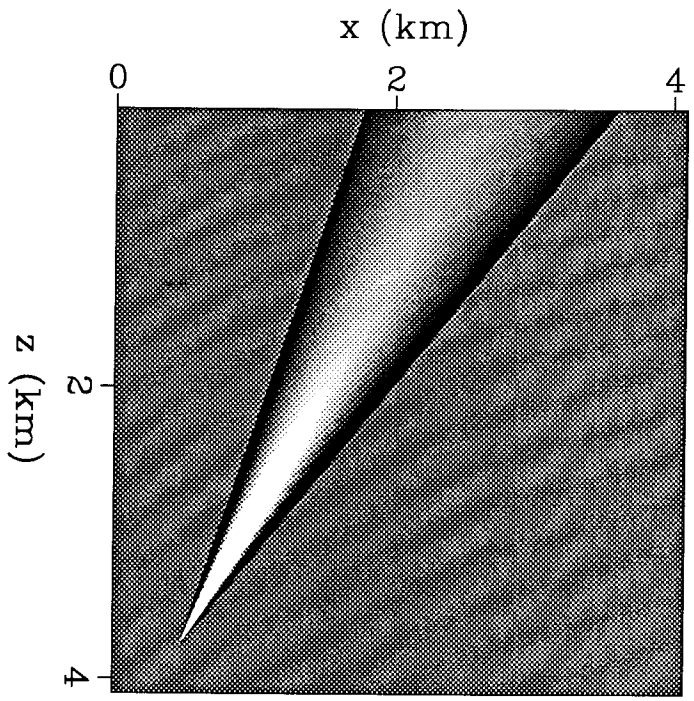

FIG. 8. The operator $\mathbf{G}_\tau$ for a single fixed reflecting point $\mathbf{d}$ and dip angle θ=30. The picture displays the magnitude of change in the migrated time location τ_d of a point $\mathbf{d}$, caused by a perturbation in the interval slowness at any other point. The point $\mathbf{d}$ is located at the apex of the triangular region. The gray background indicates no change; because of the finite cable aperture, the operator is zero outside the central triangular region. Within the triangular region, light areas indicate positive response and dark areas negative response. The operator is similar to the flat dip operator in Figure 2, but skewed by the dip.

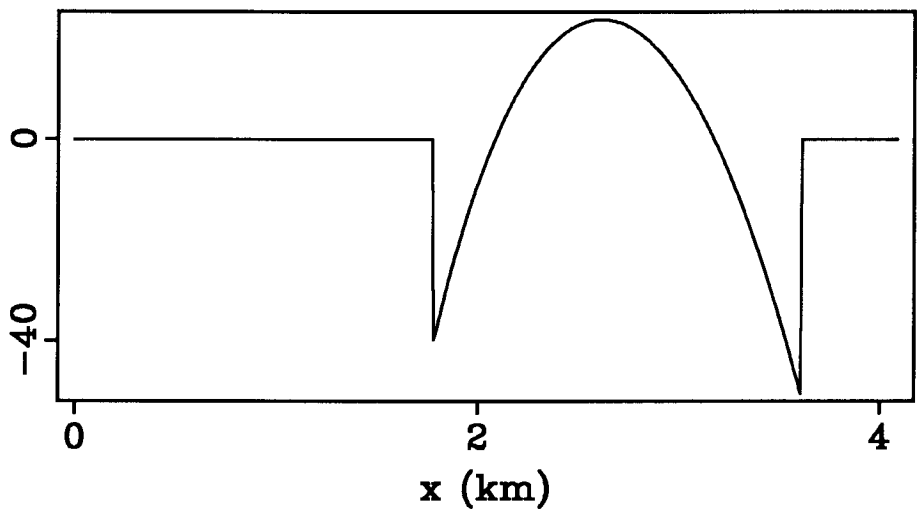

FIG. 9. Amplitude of $\mathbf{G}_\tau$ for a dipping bed, plotted as a function of lateral anomaly position x_a with anomaly depth z_a held constant. This figure corresponds to a cross-section along the top of Figure 8. Wide offset rays show a negative response, and inner offsets a positive response, similar to that for the flat bed operator in Figure 5.

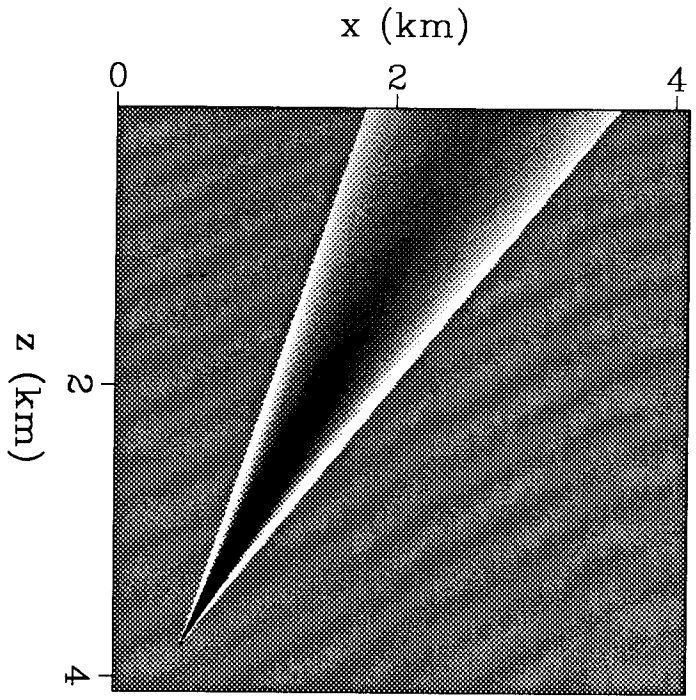

FIG. 10. The operator $\mathbf{G}_y$ for a single fixed reflecting point **d** and dip angle θ=30. The picture displays the magnitude of change in the migrated time location τ_d of a point **d**, caused by a perturbation in the interval slowness at any other point. The point **d** is located at the apex of the triangular region. The gray background indicates no change; because of the finite cable aperture, the operator is zero outside the central triangular region. Within the triangular region, light areas indicate positive response and dark areas negative response.

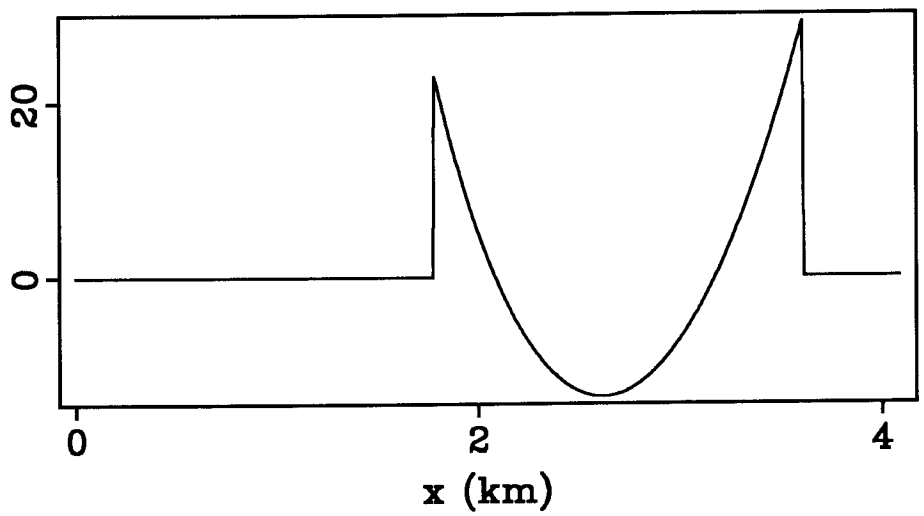

FIG. 11. Amplitude of $\mathbf{G}_\tau$ for a dipping bed, plotted as a function of lateral anomaly position x_a with anomaly depth z_a held constant. This figure corresponds to a cross-section along the top of Figure 10. Wide offset rays show a positive response, and inner offsets a negative response, proportional to the pattern for G_τ in Figure 9 but opposite in sign.

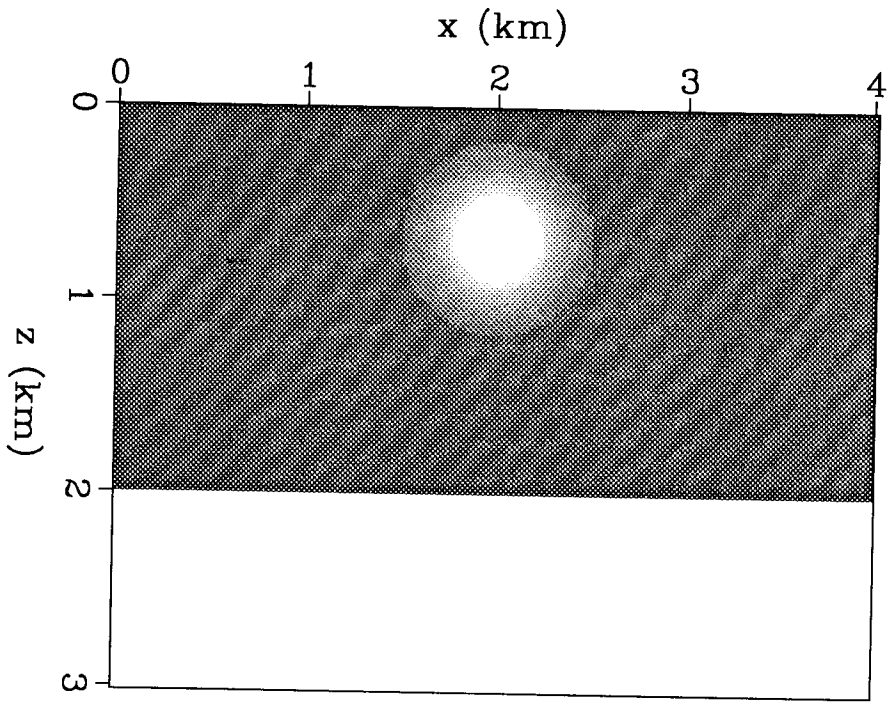

FIG. 12. Slowness model with a flat reflector and a gaussian anomaly. Slowness in the upper layer is 0.5 s/km, and in the lower layer is 0.33 s/km. The peak of the circular anomaly has a slowness of 0.476 s/km. This model was used to generate the data in Figure 13.

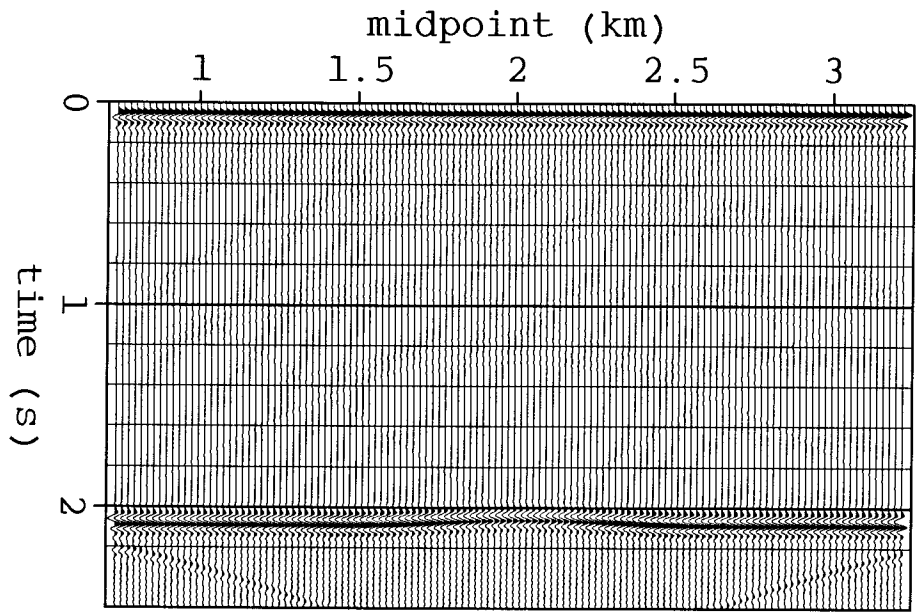

FIG. 13. Synthetic zero offset section generated by finite-difference modeling using the slowness model in Figure 12.

small time delay in the apparent location of the reflector and a concurrent change in the apparent slowness. This can be see in Figure 14; the modeled data give a slowness for the unperturbed flat bed that is a little higher than the correct value of 0.5. For best results, good spiking deconvolution and rotation to a zero-phase wavelet is probably needed before velocity analysis.

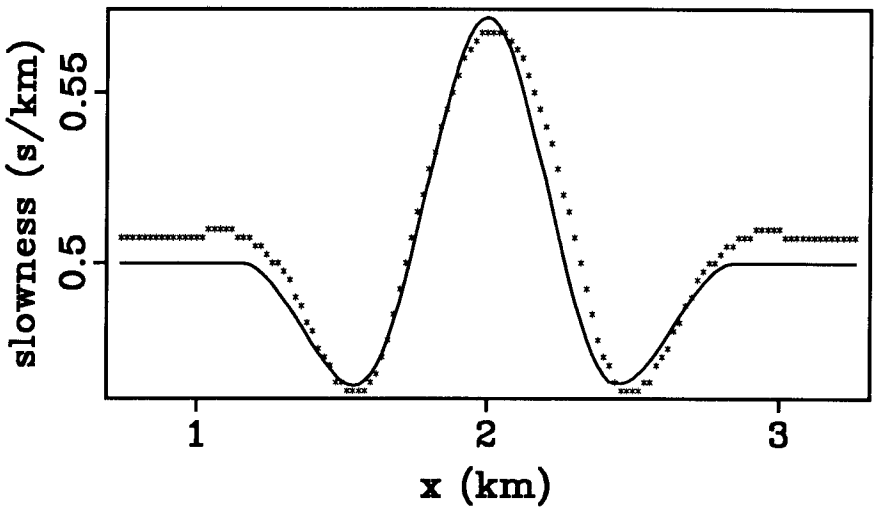

FIG. 14. Migration slownesses for the flat bed in Figure 12. The solid curve was predicted using the $\mathbf{G}_w$ operator described in this paper. The stars are values measured from processing finite-difference synthetic data.

Unfortunately, I did not get similar comparisons for dipping beds and for more complex structural models completed before the deadline for this report. I also hope to invert such results by numerical inversion of the forward linear operator to examine the resolution possible using this method. Finally, I want to use the linear operator to find a gradient direction for an iterative inversion that would allow me to move away from the assumption of constant background slowness.

CONCLUSIONS

The linear operator relating migration slownesses and interval slownesses that I described in SEP-51 (Fowler, 1987) can be understood as a filtered version of conventional tomographic back-projection. It can be implemented stably using singular value decomposition to solve for the filtering stage by inverting double-square-root traveltime equations. For flat beds this operator reduces both theoretically and numerically to Toldi's stacking slowness operator, and accurately predicts changes in migration slowness arising from perturbations in an interval slowness model. For dipping beds, the operator still resembles the flat bed one, but is skewed by the effect of the dip.

ACKNOWLEDGEMENTS

I thank Fabio Rocca for many useful discussions, and John Etgen for providing the finite-difference modeling code I used.

REFERENCES

Al-Yahya, K.M., 1987, Velocity analysis by iterative profile migration: Ph.D. thesis, Stanford University (SEP-53).

Bishop, T.N., Bube, K.P., Cutler, R.T., Langan, R.T., Love, P.L., Resnick, J.R., Shuey, R.T., Spindler, D.A., and Wyld, H.W., 1985, Tomographic determination of velocity and depth in laterally varying media: Geophysics, **50**, 903-923.

Fowler, P.J., 1984, Incorporating dip corrections in velocity analysis using constant velocity stacks: SEP-38, 113-132.

Fowler, P.J., 1985, Migration velocity analysis by optimization: linear theory: SEP-44, 1-20.

Fowler, P.J., 1986, Extending Toldi's velocity analysis algorithm to include geologic structure: SEP-48, 65-77.

Fowler, P.J., 1987, Analysis of a dip-dependent operator relating migration velocities and interval velocities: SEP-51, 63-83.

Gray, W.C., and Golden, J.E., 1983, Velocity determination in a complex Earth: Presented at the 53rd annual SEG meeting, in Las Vegas

Larner, K.L., Hatton, L., Gibson, B., and Hsu, I-C., 1981, Depth migration of imaged time sections: Geophysics, **46**, 734-750.

Loinger, E., 1983, A linear model for velocity anomalies: Geophysical Prospecting, **31**, 98-118.

Shurtleff, R.N., 1984, An F-K procedure for prestack migration and migration velocity analysis: Presented at the 46th annual EAEG meeting, in London.

Stork, C., and Clayton, R.W., 1986, Case study of traveltime tomography applied to data sets containing lateral velocity variations: Presented at the 56th annual SEG meeting, in Houston.

Sword, C.H., 1987, Tomographic determination of interval velocities from reflection seismic data: the method of controlled directional reception: Ph.D. thesis, Stanford University (SEP-55).

Toldi, J.L., 1985, Velocity analysis without picking: Ph.D. thesis, Stanford University (SEP-43).

Best Student Paper Award

for

1986 Fall Meeting

presented to

Charles H. Sword, Jr.

by the Section of

Seismology

of the

American Geophysical Union

Stewart W. Smith

PRESIDENT